Microscopic Measurements of Electrical Potential in Hydrogenated Nanocrystalline Silicon Solar Cells

Preprint

C.-S. Jiang, H.R. Moutinho, R.C. Reedy, and M.M. Al-Jassim
National Renewable Energy Laboratory

B. Yan, G. Yue, L. Sivec, J. Yang, and S. Guha
United Solar Ovonic, LLC

X. Tong
Brookhaven National Laboratory

To be presented at the 2012 MRS Spring Meeting
San Francisco, California
April 9–13, 2012

Conference Paper
NREL/CP-5200-54833
April 2012

Contract No. DE-AC36-08GO28308

Available electronically at http://www.osti.gov/bridge

Available for a processing fee to U.S. Department of Energy
and its contractors, in paper, from:

U.S. Department of Energy
Office of Scientific and Technical Information
P.O. Box 62
Oak Ridge, TN 37831-0062
phone: 865.576.8401
fax: 865.576.5728
email: mailto:reports@adonis.osti.gov

Available for sale to the public, in paper, from:

U.S. Department of Commerce
National Technical Information Service
5285 Port Royal Road
Springfield, VA 22161
phone: 800.553.6847
fax: 703.605.6900
email: orders@ntis.fedworld.gov
online ordering: http://www.ntis.gov/help/ordermethods.aspx

Cover Photos: (left to right) PIX 16416, PIX 17423, PIX 16560, PIX 17613, PIX 17436, PIX 17721

Printed on paper containing at least 50% wastepaper, including 10% post consumer waste.

Microscopic Measurements of Electrical Potential in Hydrogenated Nanocrystalline Silicon Solar Cells

C.-S. Jiang, H.R. Moutinho, R.C. Reedy, M.M. Al-Jassim
National Renewable Energy Laboratory, Golden, CO 80401, USA
B. Yan, G. Yue, L. Sivec, J. Yang, S. Guha
United Solar Ovonic LLC, Troy, MI 48084, USA
X. Tong
Brookhaven National Laboratory, Upton, NY 11973, USA

ABSTRACT

We report on a direct measurement of electrical potential and field profiles across the *n-i-p* junction of hydrogenated nanocrystalline silicon (nc-Si:H) solar cells, using the nanometer-resolution potential imaging technique of scanning Kelvin probe force microscopy (SKPFM). It was observed that the electric field is nonuniform across the *i* layer. It is much higher in the *p/i* region than in the middle and the *n/i* region, illustrating that the *i* layer is actually slightly *n*-type. A measurement on a nc-Si:H cell with a higher oxygen impurity concentration shows that the nonuniformity of the electric field is much more pronounced than in samples having a lower O impurity, indicating that O is an electron donor in nc-Si:H materials. This nonuniform distribution of electric field implies a mixture of diffusion and drift of carrier transport in the nc-Si:H solar cells. The composition and structure of these nc-Si:H cells were further investigated by using secondary-ion mass spectrometry and Raman spectroscopy, respectively. The effects of impurity and structural properties on the electrical potential distribution and solar cell performance are discussed.

1. INTRODUCTION

Electrical potential or field distribution across the junction of hydrogenated amorphous silicon (a-Si:H) and nanocrystalline silicon (nc-Si:H) solar cells is critical for the device performance [1,2]. Unlike crystalline Si (c-Si) solar cells, which commonly have a *p-n* junction structure, a-Si:H and nc-Si:H solar cells are usually designed in an *n-i-p* or *p-i-n* structure. This is because of much shorter carrier diffusion lengths [1,2] in the noncrystalline materials than in c-Si. The incorporation of an *i* layer is to expand the built-in electric field and enhance the photo-carrier collection. However, the cell efficiency is still fundamentally limited by insufficient carrier collection lengths. It is believed that when the thickness of the *i* layer is close to or exceeds the collection length, the photo-carriers cannot effectively drift away from the *i* layer. They are trapped in the *i* layer and build up space charges that lead to a nonuniform electric field distribution. In addition, unintentional impurities in the *i* layer also make the electric field profile deviate significantly from uniform distribution [3,4] and reduce the effectiveness of carrier collection. Therefore, information about the electric field distribution in the *i* layer is a key factor for understanding the device physics.

There are many theoretical modeling studies on the potential distribution in thin-film solar cells [1,2,4]. However, experimental characterizations of the potential have been limited to indirect measurements. Most techniques are unable to directly deduce the spatial distribution of potential across the *n-i-p* junction. We have achieved real-space nm-resolution measurement of the electrical potentials using scanning Kelvin probe force microscopy (SKPFM) [5–7] and successfully used this technique to characterize c-Si solar cells [6] and a-Si:H solar cells [7]. In this work, we report on the electrical potential/field distributions of nc-Si:H solar cells.

2. EXPERIMENTAL

The nc-Si:H solar cells were deposited on GaAs wafer substrates for the cross-sectional cleaving [7]. A Ag/ZnO back reflector was deposited on the GaAs wafer as the back contact and for light trapping. Details of the nc-Si:H solar cell depositions were published elsewhere [8]. For both atomic force microscopy (AFM) and SKPFM imaging, a flat cross-section of solar cell is necessary. The GaAs wafer can be cleaved atomically flat, and the nc-Si:H device deposited on it can be relatively flat, as well. The current density versus voltage (J-V) characteristics of solar cells was measured under an AM1.5 solar simulator at 25°C; quantum efficiencies (QE) were measured under zero and -3.0-V electrical biases. The difference in QE curves under these two conditions was used to determine the QE loss. Three nc-Si:H single-junction solar cells were studied. Sample A was made at a low deposition rate of 0.65 nm/s. It has a reasonably good performance as shown in Table I. Sample B was deposited at a high deposition rate of 1.30 nm/s. The cell performance of Sample B is not as good as Sample A. Sample C was also deposited at a low rate of 0.50 nm/s in a condition such that the impurity levels are higher than the other two samples.

SKPFM is based on the non-contact mode of AFM (Termomicroscope CP). It uses the low-frequency mode (~20 kHz) rather than the second-harmonic frequency, because the cross-sectional surface has a corrugation of ~300 nm, which would incorporate a significant topographic effect if the second-harmonic mode is used. This low-frequency mode gives an energy resolution of ~50 meV. The AC voltage amplitude is 2 V. The tip/sample separation or the tip oscillation amplitude setting is 10 nm. Commercial PtIr-coated Si tips were used (Olympus AC240TM). In addition, secondary-ion mass spectrometry (SIMS) and Raman spectroscopy were employed to investigate the effects of impurity and structure on nc-Si:H cell performance. The Raman measurements were made by using a confocal Raman microscopy (WITec alpha 300) with a 532-nm laser as the excitation source.

3. RESULT AND DISCUSSION

Table I lists the J-V and QE parameters of the three samples, where the J_{sc} is calculated from integral of QE curves measured under zero bias and the AM1.5 solar spectrum. The ΔQE is calculated from the integral of [QE(-3.0V)-QE(0V)]/QE(-3.0V) and the AM1.5 solar spectrum from 610 to 1200 nm. Comparing Samples A and B, one may see that all of the three parameters of short-circuit current density (J_{sc}), open-circuit voltage (V_{oc}), and fill factor (FF) are reduced by the increase of deposition rate. Comparing Samples A and C, one may see that although the overall performance is similar, Sample C has a larger QE loss. Figure 1 shows the (a) QE spectra measured under zero bias and (b) QE loss spectra, where the QE loss is the relative difference between the QEs measured under 0 and -3 V. The QE losses in Samples A and B are about 2%–4% in the long-wavelength region of λ>610 nm, while Sample C shows a high loss of 8%–9%.

Table I. Solar cell performance parameters of the three nc-Si:H cells.

Sample	*Efficiency* (%)	J_{sc} (mA/cm^2)	*ΔQE*(>610 nm) (%)	V_{oc} (V)	*FF*
A	8.58	25.35	3.6	0.528	0.641
B	7.06	22.82	3.7	0.518	0.597
C	8.66	25.01	7.4	0.546	0.634

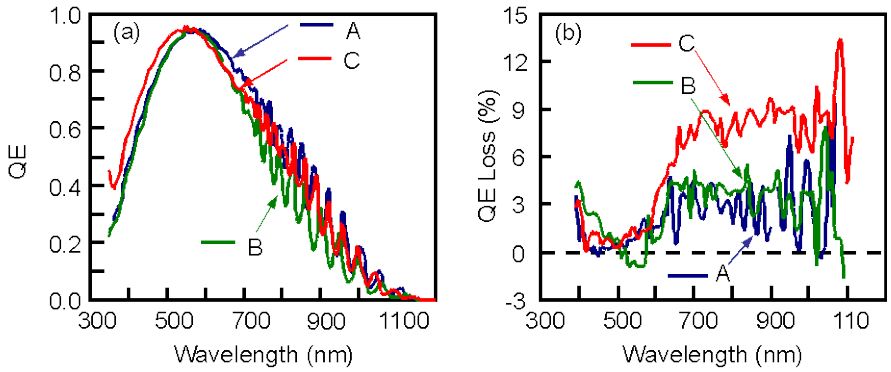

Fig. 1. (a) QE and (b) QE loss spectra of the three nc-Si:H cells.

Figures 2(a) and 2(b) show an AFM topographic and the corresponding SKPFM potential images taken on Sample A with a bias of V_b = -1 V. The device structure is illustrated on the left side of Fig. 2(a). The corrugation and potential profiles in Fig. 2(c) are averages of the corresponding images along the lateral direction. From the potential profile, one sees that the potential on the Ag and ZnO is lower than on the *n*-side of nc-Si:H and the GaAs substrate, due to different workfunctions of the materials [7]. The potential on the *n*-side of *i* layer is relatively flat, and it decreases approaching the *p* layer (a negative bias is applied to the *p*-side). Because the SKPFM measures surface potential of the sample, the potential image and profile in Fig. 2 are affected by the trapped charges on the cross-sectional surface. Therefore, the measured potential profile is not necessarily identical with the potential in the bulk of device. To obtain the potential distribution in the bulk, we have developed a procedure to deduce the change of the potential in the bulk with V_b, by measuring the change in surface potential [6,7]. Because the surface charge configuration should not change significantly with a small V_b =~1–2 V, the change in surface potential as measured by SKPFM should be identical with that in the bulk. We have used this procedure for determining *p*-*n* junction locations in c-Si and Cu(In,Ga)Se_2 solar cells [6].

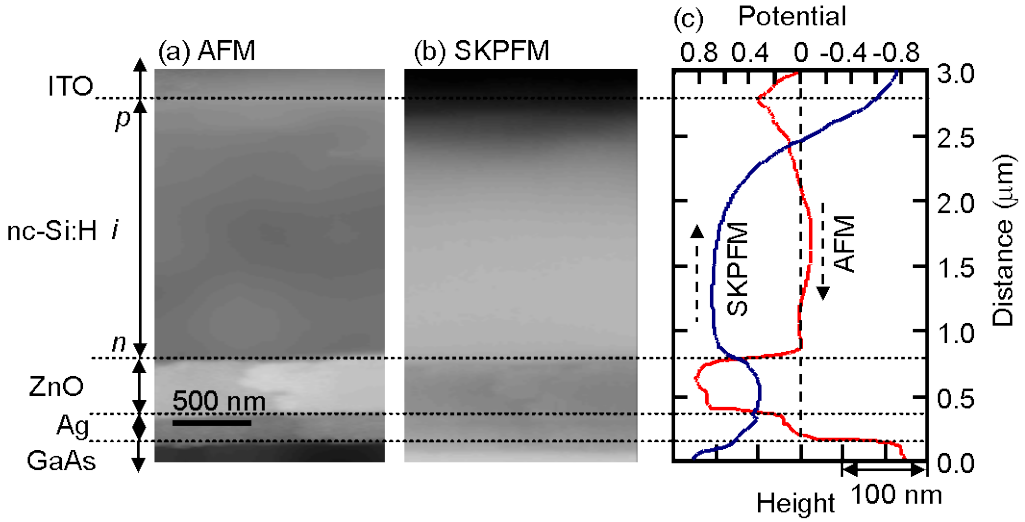

Fig. 2. (a) AFM topographic and (b) the corresponding SKPFM potential images taken on the cross-section of nc-Si:H cell Sample A. Profiles in (c) are averages of the corresponding images along the lateral direction.

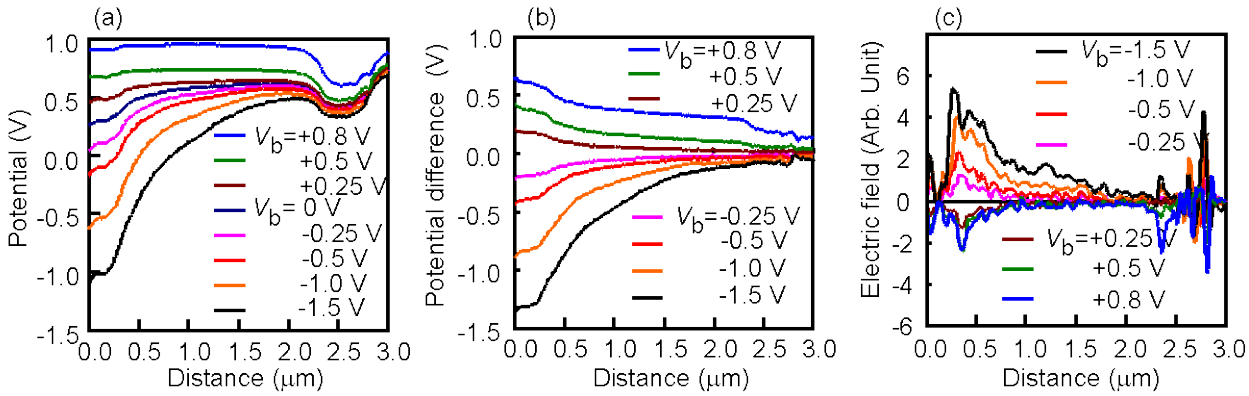

Fig. 3. (a) Potential profiles measured under various biases on the junction of Sample A, (b) the

Figure 3(a) shows the potential profiles measured with different V_b values, in which each profile is an average of 64 potential lines. Figure 3(b) shows the potential differences measured under various biases and $V_b = 0$. As shown in Fig. 3(c), the V_b-induced changes in the electric field were deduced by taking derivatives of the potential changes. One sees that the potential change in Fig. 3(b) and the corresponding field change in Fig. 3(c) are highly nonuniform. The electric field is high on the *p*-side and it decreases moving toward the *n*-side. The noise of electric field in the back reflector and front contact is due to the rough cross-sectional topography. The field distribution in nc-Si:H is different from that of the a-Si:H cell, where the field is through the whole *i* layer and higher on both *n*- and *p*-sides than in the middle of the *i* layer [7].

Figure 4 compares the electric field distributions of the three samples. Sample B has a more nonuniform distribution than Sample A as indicated by the higher peak at the *p/i* interface and the faster decay. The enhanced nonuniformity in the electric field distribution by the high deposition rate could contribute in part to the difference in cell performance as listed in Table I. Sample C has an even more pronounced nonuniform electric field distribution than Samples A and B. The electric field is very low in the regions near the *n* layer and in the middle of the *i* layer. As we proposed previously, a large long-wavelength QE loss could be caused by weak electric field distribution in the *n*-side of the *i* layer [9]. The result of Fig. 4(c) proves our hypothesis. The weak electric field in the *n*-side of the *i* layer is normally caused by *n*-type doping in the *i* layer [9]. Therefore, impurity measurement is important to further support the hypothesis.

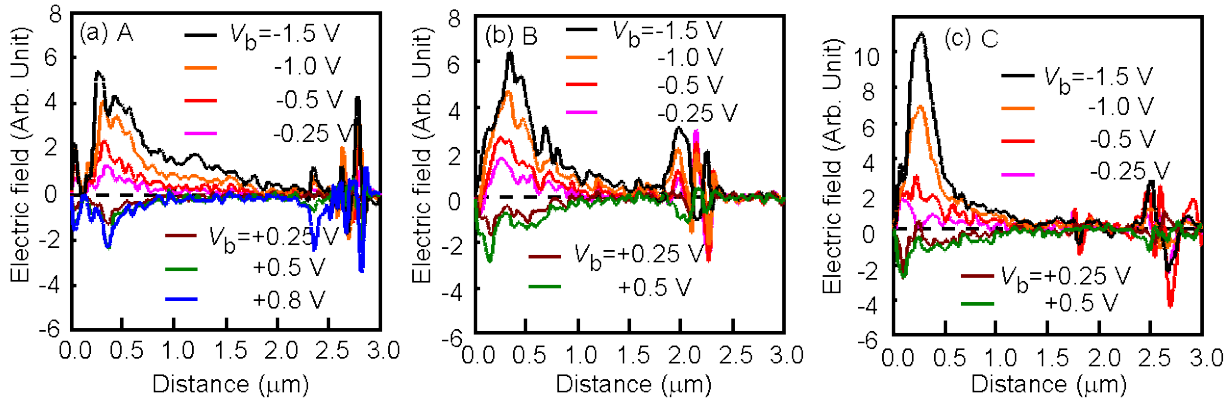

Fig. 4 (a), (b), and (c): V_b-induced changes in the electric field across the *n-i-p* junctions of Samples A, B, and C, respectively.

Figure 5 shows SIMS impurity profiles of H, O, C, P, and B across the *i* layer of Sample A and Sample C. The H and P concentrations in the two cells are similar. However, O, C, and B concentrations in Sample C are significantly higher than in Sample A. The *i* layer of nc-Si:H solar cells usually shows slightly *n*-type characteristics [3,4], which is caused by unintentional impurities such as O. Oxygen in Si is commonly believed to be thermal double donors [10]. The four times higher O contamination (~2.7×10^{19}/cm^3) in Sample C than in Sample A is likely the cause for the more pronounced nonuniform electric field in Sample C than in Sample A. Comparing Figs. 4 and 5, we can conclude that the electric field and SIMS measurements are consistent and support our previous hypothesis very well [9]. We need to point out that the B concentration is also higher in Sample C than in Sample A. From our previous study, we found that small amounts of B doping can compensate O impurity and reduce the long-wavelength QE loss. Excessive B concentration can cause a short-wavelength loss. Because a large long-wavelength QE loss is observed in Sample C, we believe that the amount of B in Sample C is not high enough to compensate the O impurity. Further, if the B concentration in Sample C was as low as in Sample A, we would expect a much higher long-wavelength QE loss in Sample C than observed in Fig. 1(b).

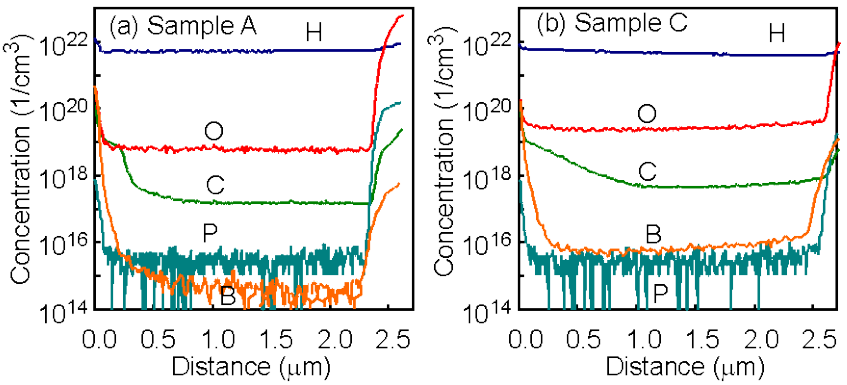

Fig. 5. Impurity profiles of Samples A and C measured by SIMS.

Figure 6 shows Raman spectra measured on the three samples, which are normalized by the crystalline peak at ~510–520 cm^{-1}. From the Si-Si TO vibration mode, one notes that Sample A has a slightly higher crystalline volume fraction (ρ_c) than sample C. This is one reason why Sample C has a higher V_{oc} than Sample A. Although Sample C has higher impurity levels than Sample A, the other structural defects such as dangling bonds may not be high, which leads to a reasonable FF. Comparing Sample B to the others, it has a much low ρ_c, which results in the low J_{sc}. One may expect to see a higher V_{oc} in Sample B, but a high defect density and wide bandtails may reduce the V_{oc}. The difference in the electric field distribution between Samples A and B, as shown in Fig. 4, could be caused by different defect densities instead of impurities.

The electric field in nc-Si:H *n-i-p* solar cells is highly nonuniform, with a high electric field near the *p/i* interface and a low electric field in the *n*-side. From an overall picture, the electric field distribution in nc-Si:H solar cells is in between c-Si and a-Si:H solar cells. In c-Si solar cells, the main absorbing layer is weakly doped, and the emitter and back surface field layers are heavily doped. Therefore, the electric field is mainly located in a narrow depletion region. The

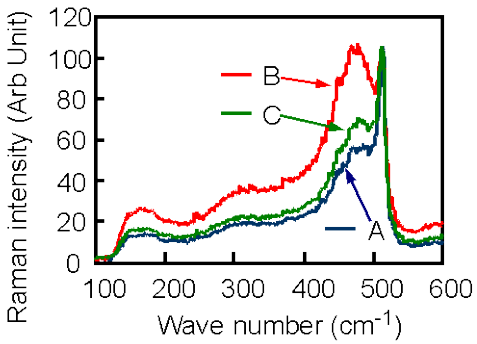

Fig. 6. Raman spectra measured on the three nc-Si:H cells.

carrier transport in the absorber is through diffusion. In a-Si:H solar cells, the electric field crosses the whole *i* layer with some nonuniformity and the carrier transport in the *i* layer is mainly through drift by electric field. In nc-Si:H solar cells, because of the sensitivity of forming weak donors from O, the nc-Si:H *i* layer normally shows weak *n*-type conductivity. Therefore, the electric field is much higher in the region near the *p* layer than near the *n* layer, which makes the carrier transport become a mixture of drift and diffusion. Experimentally, we observed that the diode ideality factor is around 1.2–1.3, which is close to that of diffusion-limited diodes.

4. SUMMARY

The electrical potential or electric field distribution across the *n-i-p* junction of nc-Si:H solar cells was directly measured by using SKPFM. We found that the electric field was highly nonuniform across the *n-i-p* junction—much higher on the *p*-side than in the middle and on the *n*-side of the *i* layer. This is consistent with the argument that the *i* layer is slightly *n*-type. Further, a nc-Si:H solar cell with a high QE loss shows a high oxygen concentration and a much more pronounced nonuniform distribution of the electric field. These results provide clear and direct proof of our previous hypothesis that the long-wavelength QE loss is caused by the weakening of the electric field in the *n*-side of the *i* layer. The high nonuniformity of the electric field implies that the carrier transport in nc-Si:H solar cells is a mixture of diffusion and drift by the electric field. This carrier transport picture is consistent with the dark I-V measurements, where an ideality factor around 1.2–1.3 is observed. The small ideality factor is an indication of diffusion transport of carriers across the junction.

ACKNOWLEDGEMENTS

The work at NREL was supported by the U.S. DOE under Contract No. DE-AC36-08GO28308. The work at United Solar was supported by the U.S. DOD through the U.S. Army under Subcontract No. W9132T-11-C-0007 and by the DOE through the SAI Program under Subcontract FC36-07 GO 17053. The work at the Center for Functional Nanomaterials, Brookhaven National Laboratory, is supported by the DOE, Office of Basic Energy Sciences, under Contract No. DE-AC02-98CH10886.

REFERENCES

[1] E.A. Schiff, *Sol. Energy Mater. Sol. Cells* **78**, 567 (2003).
[2] E.A. Schiff, *Mater. Res. Soc. Symp. Proc.* **1153**, 1151-A15 (2009).
[3] D. Fischer and A.V. Shah, *Appl. Phys. Lett.* **65**, 986 (1994).
[4] K. Dairiki, A.Yamada, and M. Konagai, *Jpn. J. Appl. Phys.* **40**, 486 (2001).
[5] M. Nonnemacher, M.P. O'Boyle, and H.K. Wickramasinghe, *Appl. Phys. Lett.* **58**, 2921 (1991).
[6] C.-S. Jiang, H.R. Moutinho, R. Reedy, M.M. Al-Jassim, and A. Blosse, *J. Appl. Phys.* **104**, 104501 (2008).
[7] C.-S. Jiang, A. Ptak, B. Yan, H.R. Moutinho, J.V. Li, and M.M. Al-Jassim, *Ultramicroscopy* **109**, 952 (2009).
[8] B. Yan, G. Yue, J. Yang, and S. Guha, *Mater. Res. Soc. Symp. Proc*. **989**, 335 (2007).
[9] G. Yue, B. Yan, L. Sivec, Y. Zhou, J. Yang, and S. Guha, *Sol. Energy Mater. Sol. Cells*, submitted (2012).
[10] C.A.J. Ammerlaan, in *Properties of Crystalline Silicon,* ed. R. Hull (INSPEC, London, 1999), p.663.